Original Article

High Wall Shear Stress Is Related to Atherosclerotic Plaque Rupture in the Aortic Arch of Patients with Cardiovascular Disease: A Study with Computational Fluid Dynamics Model and Non-Obstructive General Angioscopy

Keisuke Kojima[1], Takafumi Hiro[1], Yutaka Koyama[1], Akihito Ohgaku[1], Hidesato Fujito[1], Yasunari Ebuchi[1], Riku Arai[1], Masaki Monden[1], Suguru Migita[1], Tomoyuki Morikawa[1], Takehiro Tamaki[1], Nobuhiro Murata[1], Naotaka Akutsu[1], Toshihiko Nishida[1], Daisuke Kitano[1], Mitsumasa Sudo[1], Daisuke Fukamachi[1], Shunichi Yoda[1], Tadateru Takayama[2], Atsushi Hirayama[1, 3] and Yasuo Okumura[1]

[1] Division of Cardiology, Department of Medicine, Nihon University School of Medicine, Tokyo, Japan.
[2] Division of General Medicine, Department of Medicine, Nihon University School of Medicine, Tokyo, Japan.
[3] Department of Cardiology, Osaka Police Hospital, Osaka, Japan.

Aims: Wall shear stress (WSS) has been considered a major determinant of aortic atherosclerosis. Recently, non-obstructive general angioscopy (NOGA) was developed to visualize various atherosclerotic pathologies, including *in vivo* ruptured plaque (RP) in the aorta. However, the relationship between aortic RP and WSS distribution within the aortic wall is unclear. This study aimed to investigate the relationship between aortic NOGA-derived RP and the stereographic distribution of WSS by computational fluid dynamics (CFD) modeling using three-dimensional computed tomography (3D-CT) angiography.

Methods: We investigated 45 consecutive patients who underwent 3D-CT before coronary angiography and NOGA during coronary angiography. WSS in the aortic arch was measured by CFD analysis based on the finite element method using uniform inlet and outlet flow conditions. Aortic RP was detected by NOGA.

Results: Patients with a distinct RP showed a significantly higher maximum WSS value in the aortic arch than those without aortic RP (56.2 ± 30.6 Pa vs 36.2 ± 19.8 Pa, $p = 0.017$), no significant difference was noted in the mean WSS between those with and without aortic RP. In a multivariate logistic regression analysis, the presence of a maximum WSS value more than a specific value was a significant predictor of aortic RP (odds ratio 7.21, 95% confidence interval 1.78-37.1, $p = 0.005$).

Conclusions: Aortic RP detected by NOGA was strongly associated with a higher maximum WSS in the aortic arch derived by CFD using 3D-CT. The maximum WSS value may have an important role in the underlying mechanism of not only aortic atherosclerosis, but also aortic RP.

Key words: Atherosclerotic ruptured plaque, Aortic arch, Computational fluid dynamics, Non-obstructive general angioscopy, Wall shear stress

Introduction

Wall shear stress (WSS) is a tangential force generated from blood flow on the endothelial surface of blood vessels[1]. WSS has been considered as one of the most significant hemodynamic forces within the blood vessel wall. Since WSS is involved in the endothelial function, WSS significantly influences site-specific susceptibility and progression of atherosclerosis[2]. Regarding the coronary artery, previous studies have suggested that WSS affects local plaque morphology or vulnerability[3, 4] and its progression[5] and was

related to future adverse cardiac events[6, 7]. Furthermore, several studies have reported the mechanisms of the formation of aortic aneurysms or dissection mediated by WSS[8, 9].

Postmortem pathological studies have shown objective ways of evaluating aortic atherosclerosis to assess aortic plaque vulnerability, thrombi, and ruptured plaque (RP)[10, 11]. Coronary imaging modalities (intravascular ultrasound, optical coherence tomography, or coronary angioscopy) can evaluate plaque morphologies in detail[12]; however, because of the limited time or space resolution of the imaging systems, conventional imaging modalities for the aorta such as computed tomography (CT), magnetic resonance imaging (MRI), or transesophageal echocardiography could not reveal the RP. Therefore, examining the *in vivo* process of aortic atherosclerosis in detail has been difficult.

Recently, a novel method using non-obstructive general angioscopy (NOGA) was developed as a clinically feasible imaging tool for observing aortic atherosclerosis *in vivo*[13-15]. NOGA provides real-time images of the aortic wall using 6000 lights fibers within a catheter diameter of 0.75 mm, which clearly detects atherosclerotic changes and plaque vulnerability of the aortic wall in more detail than conventional imaging modalities[13]. Komatsu *et al.* documented that NOGA could detect fair amounts of aortic ruptured plaques (RP) as well as scattered cholesterol crystals from the rupture cavity in patients with cardiovascular disease. Moreover, it has been suggested that these pathological phenomena might be related to atheromatous embolization and even the formation of aortic aneurysms or dissection[13]. However, the relationship between RP and WSS distribution within the aortic wall has not been elucidated yet.

With the aforementioned gap in research, this study aimed to examine the effect of WSS on the presence of RP in the aortic arch evaluated by NOGA in patients who underwent cardiac catheterization.

Aim

This study aimed to investigate the relationship between aortic NOGA-derived RP and the stereographic distribution of WSS by using computational fluid dynamics (CFD) modeling on three-dimensional computed tomography (3D-CT) angiography.

Methods

Study Design and Subjects

This study was a single-center, retrospective observational study of 45 consecutive patients with confirmed or suspected coronary artery disease, who underwent 3D-CT as well as coronary angiography and NOGA for the aortic arch in Nihon University Itabashi Hospital between March 2015 and September 2019. We excluded patients with acute coronary syndrome, cardiogenic shock, acute aortic syndrome, aortic aneurysm with thoracic aorta diameter of >6 cm and abdominal aorta diameter of >5 cm, cerebral infarction in acute phase, hemodialysis, uncontrollable hypertension, allergy to contrast media, and pregnancy. Because of inadequate blood flow clearance or access limitation due to severe aortic or arterial angulation, patients without good imaging qualities for NOGA of the whole aortic arch were also excluded. Although NOGA can be used under regular health insurance system in Japan, this study was performed after informed consent was obtained from each patient. The Institutional Review Committee of Nihon University Itabashi Hospital approved this study protocol (RK-180710-18). This study proceeded in accordance with the Declaration of Helsinki.

Acquisition and Measurement of the Aortic Arch with 3D-CT Angiography (Supplemental Fig. 1)

Aortic CT angiography was performed using 320-detector row scanners (Aquilion ONE Vision; Canon Medical Systems Corp., Tokyo, Japan). Iodinated contrast medium (Iomeron®; Bracco-Eisai Co., Ltd., Tokyo, Japan) was administered to all patients at 400 mg of iodine/kg with an injector, with scan parameters as follows: collimation, 1 mm; rotation time, 0.5 sec; tube voltage, 120 kV; and tube current (mA) calculated with the automatic exposure control technique. Stereographic reconstruction of the aortic luminal architecture was performed by 3D-CT using a commercially available workstation (INTAGE Volume Editor ver 1.2; Cybernet Systems Co., Ltd., Tokyo, Japan)[6]. In this study, the aorta of interest was determined from the proximal (within the ascending aorta) to the distal (within the descending aorta) horizontal planes at the same height of the bifurcation carina of the pulmonary artery. The diameter of the proximal and distal horizontal planes at aortic cross-sectional lumens, the center lumen line (CLL) length along the aortic longitudinal lumen, the radius of the inner curvature (R-inc) of the aorta, the aortic arch tortuosity index (=CLL / R-inc), and the maximum diameter of the aortic arch of interest were measured[16].

Calculation and Color Mapping of WSS

In this study, color mapping of WSS was performed using a previously reported modified
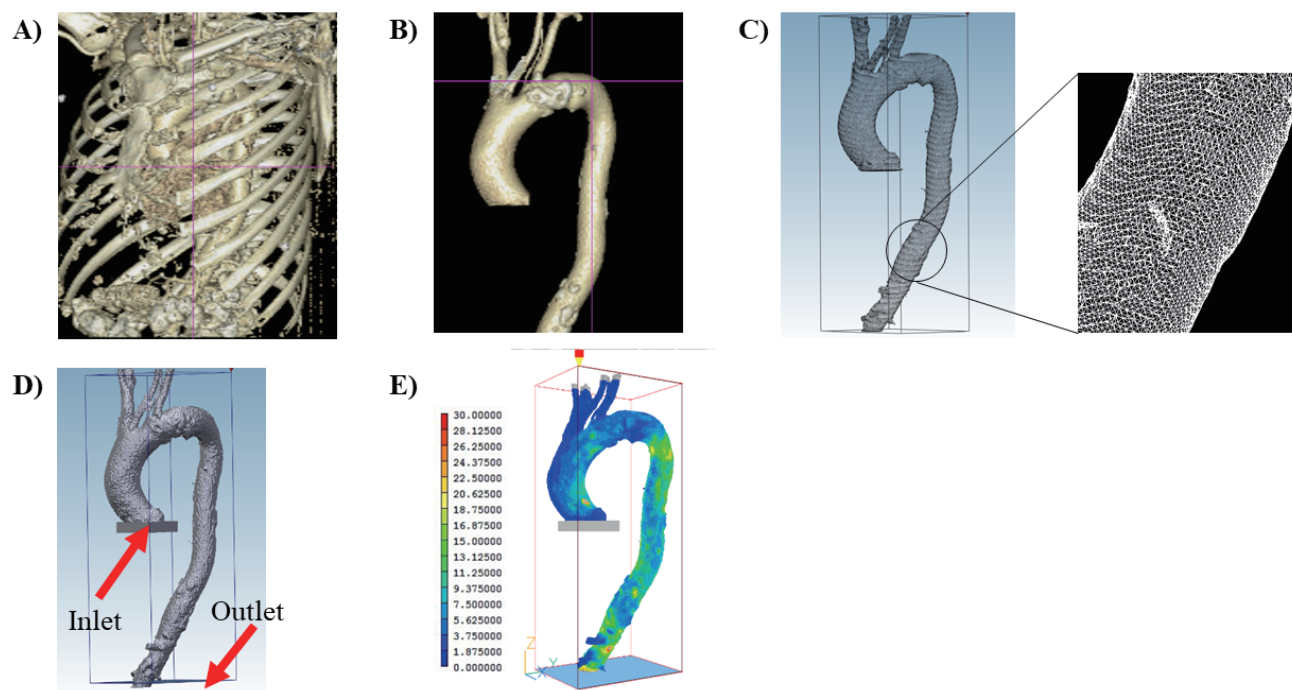
Fig. 1. Quantification of WSS in the aortic arch using CFD modeling on 3D-CT

(A) Initial reconstructed volume-rendered image of the whole body trunk. (B) The aorta was clipped from other tissue and extracted. (C) The aorta was applied to define a mesh polygon structure that was used for the analysis of CFD. (D) The CFD analysis was performed to calculate the distribution of WSS by using uniform inlet and outlet flow conditions. (E) Color mapping of the WSS distribution was then performed. CFD, computational fluid dynamics; WSS, wall shear stress

method[17]. Three-dimensional reconstruction of the aortic lumen was applied to define a mesh polygon structure that was used for the analysis of CFD **(Fig. 1)**. CFD analysis has been conducted to calculate the distribution of blood flow velocity to reveal the three-dimensional distribution of WSS inside the lumen of the aortic arch using commercially available application (PHOENICS-CFD Works ver 4.3.6.1.; Concentration Heat and Momentum Limited, London, UK) based on the finite element method using uniform inlet and outlet flow pre-calculation conditions[4, 6-8]. The spatial resolution of the subunits was approximately 0.01 mm^2. The aortic wall was divided into two areas, which roughly corresponded to the greater and lesser curvature areas, respectively. In this study, the Reynolds number was also calculated. Reynolds number is originally a parameter to distinguish turbulent flow from laminar flow in a duct as determined by physics[18]. In the calculation of CFD, several pre-calculation conditions were assumed in this study, including constant laminar flow, uniform stationary inflow with a velocity of 60 cm/sec at the aortic root of the entrance, the absence of flow resistance at the outlet, and the absence of flow slip on the aortic wall. Intravascular flow parameters were shown by

solving the transport equations governing the conservation of mass and momentum[19]. Additionally, we assumed that the aortic wall was solid and that the blood was incompressible, homogeneous, and Newtonian[20], with a density of 1050 kg/m^3 and a viscosity of 0.003 PaS[21]. The hemodynamic factors including blood pressure, pulse pressure, and heart rate at the measurement of WSS were also measured.

Cardiac Catheterization and Angioscopic System

Catheterization was performed in a standard technique via the femoral artery with a 6-F sheath and guiding catheter. NOGA examination of the aorta was performed just after coronary angiography using a commercially available system with a VISIBLE Fiber (FT-203F, Fiber Tech Co., Ltd., Tokyo, Japan), a fiber imaging system, and a console (InterTec Medicals Co., Ltd., Osaka, Japan)[13]. The white balance was adjusted for color correction before observation. NOGA images were recorded on a digital video recorder for off-line analysis. Observations were made while the blood was cleared away from view to infuse low-molecular-weight dextran with the dual infusion method as shown in a previous report[22]. The tips of the fiber catheter, a 4-F probing catheter, and the guiding cath-

eter were set at the same position, and these catheters were pulled back from the ascending aorta to the descending aorta and rotated for scanning of the whole aortic wall[13-15, 23].

Angioscopic Observation of the Aortic Arch

The number and presence as well as distribution of atherosclerotic plaque, RP, yellow plaque, and thrombi in the aortic arch were assessed by NOGA. Furthermore, the maximum yellow grade of the plaques was also evaluated. RP was defined as puff rupture or puff-chandelier rupture having a scattered "puff"-like appearance according to previous reports[14, 23]. Yellow grade was defined as "4 points-scale grading" which was reported previously[23]. The yellow plaque was defined as the yellow grade of 2 or 3. We localized the site of RP with reference to the vertebral bodies, the bifurcation of the pulmonary trunk, and branches of the arteries using dual fluoroscopic system of two different directions; its corresponding area was carefully identified within the aortic arch image of the color-coded 3D-CT for WSS. These evaluations were performed by two angioscopy specialists who were blinded to the patient clinical status.

Statistical Analysis

Continuous variables were expressed as mean ± standard deviation for normally distributed variables and as median (25–75th percentiles) for non-normally distributed variables and were compared using a Student's t-test and a Mann-Whitney U-test, respectively. The Wilcoxon test was used for ordinal variables. Categorical variables were expressed as frequencies and analyzed using chi-square statistics or Fisher's exact test. A significance level of 0.05 was used, and two-tailed tests were applied. The receiver operating characteristic (ROC) curve was plotted to identify the maximum cutoff values of WSS value to predict the presence of aortic RP. Logistic regression analysis was performed to assess the predictors of aortic RP using independent variables, which were applied as significant risk factors for the presence of the aortic RP in a previous report[14]. JMP statistics 12.2.0 (SAS Institute, Cary, NC, USA) was used for all statistical analyses.

Results

Study Patients

This study recruited 45 patients with a mean age of 69 ± 10 years (range, 45–86 years). All study patients had atherosclerotic plaques of the aortic arch. The aortic RP and yellow plaque were detected in 25 patients (56%) and 22 patients (49%), respectively

Table 1. The findings of NOGA-derived atherosclerotic plaques of the aortic arch

NOGA findings	
Number of ruptured plaques	1 [0-2]
Number of yellow plaques	2 [1-4]
Number of thrombi	1 [0-2]
Max yellow plaque grade	2 [2-3]
Presence of atheromatous plaques	45 (100)
Presence of ruptured plaques	25 (56)
Presence of yellow plaques	22 (49)
Presence of thrombi	28 (62)

Data are presented as n (%) or median [interquartile range]. The yellow plaque was defined as the yellow grade of 2 or 3. NOGA, non-obstructive general angioscopy.

(Table 1). Baseline demographics are shown in **Table 2**. No significant differences in age, gender, hemodynamic factors (blood pressure, pulse pressure, and heart rate), atherosclerotic risk factors, comorbidities, lipid profile, inflammatory marker, renal function, and medications were found between patients with and without aortic RP. No complications due to NOGA observation occurred during NOGA examination or for 48 h after the procedure.

Relationships between the Presence of RP and CFD Findings of the Aortic Arch

The 3D-CT and CFD findings of the study population are shown in **Table 3**. No significant difference was found in CT parameters which represented morphological features of the aortic arch between patients with and without aortic RP. As regards CFD findings, patients with aortic RP had a significantly higher maximum WSS value than those without aortic RP (with aortic RP vs. without aortic RP; 56.2 ± 30.6 Pa vs. 36.2 ± 19.8 Pa, $P = 0.017$), although no significant difference was found in the mean WSS value between the two groups. Furthermore, in both the greater and lesser curvature areas of the aortic arch, patients with aortic RP had a significantly higher maximum WSS value than those without aortic RP (with aortic RP vs. without aortic RP in the greater curvature, 43.2 ± 26.2 Pa vs. 28.1 ± 15.8 Pa, $P = 0.032$; in the lesser curvature, 51.7 ± 29.7 Pa vs. 32.5 ± 18.2 Pa, $P = 0.018$), although no significant differences were noted in the mean WSS value between the groups (Fig. 2). Representative images of color mapping of WSS and NOGA findings of the aortic arch are presented in **Fig. 3**.

Table 2. Baseline characteristics

	All patients $N=45$	Presence of Ruptured plaques $N=25$	Absence of Ruptured plaques $N=20$	P value
Age (yrs)	69 ± 10	71 ± 9	65 ± 11	0.053
Gender(male)	41 (91)	22 (88)	19 (95)	0.12
BSA (m²)	1.68 ± 0.17	1.66 ± 0.18	1.72 ± 0.16	0.30
BMI	23.3 ± 3.3	23.2 ± 3.4	23.4 ± 3.2	0.85
Systolic BP (mmHg)	130 ± 24	127 ± 25	134 ± 23	0.48
Diastolic BP (mmHg)	68 ± 12	65 ± 11	71 ± 12	0.21
Heart Rate (bpm)	69 ± 12	68 ± 13	71 ± 12	0.49
Pulse pressure (mmHg)	65 ± 25	67 ± 30	63 ± 23	0.74
LVEF (%)	65 ± 11	67 ± 10	62 ± 11	0.10
Atherosclerotic risk factors				
Diabetes Mellitus	16 (36)	10 (40)	6 (30)	0.56
Dyslipidemia	34 (76)	20 (80)	14 (70)	0.62
Hypertension	30 (67)	17 (68)	13 (65)	0.98
Chronic kidney disease	10 (22)	6 (24)	4 (20)	0.89
Comorbidities				
Coronary artery disease	28 (62)	16 (64)	12 (60)	0.95
Old myocardial infarction	13 (29)	7 (28)	6 (30)	0.80
Stroke	12 (27)	5 (20)	7 (35)	0.22
Peripheral artery disease	6 (13)	4 (16)	2 (10)	0.60
Heart failure	4 (9)	1 (5)	3 (12)	0.18
Laboratory data				
Creatinine (mg/dl)	0.84 [0.77-0.94]	0.85 [0.80-0.95]	0.80 [0.65-0.95]	0.38
eGFR (ml/min/1.73m²)	72.2 ± 21.8	67.4 ± 20.3	79.0 ± 22.7	0.086
HbA1c (%)	6.5 ± 1.1	6.3 ± 0.9	6.8 ± 1.3	0.12
Total-Cholesterol (mg/dl)	176 ± 43	174 ± 43	182 ± 46	0.67
HDL-Cholesterol (mg/dl)	43 ± 12	42 ± 13	44 ± 12	0.71
LDL-Cholesterol (mg/dl)	105 ± 35	105 ± 36	104 ± 33	0.96
Triglyceride (mg/dl)	156 ± 95	136 ± 69	184 ± 118	0.099
hs-CRP (mg/dl)	0.13 [0.05-0.36]	0.14 [0.05-0.39]	0.11 [0.06-0.34]	0.30
Uremic Acid (mg/dl)	5.8 ± 1.2	5.7 ± 0.9	6.0 ± 1.5	0.43
NT-pro BNP (pg/dl)	150 [57-696]	195 [59-716]	128 [57-964]	0.87
Medications				
Statin	32 (71)	18 (72)	14 (70)	0.90
Aspirin	31 (69)	18 (72)	13 (68)	0.80
Dual anti-platelets	24 (53)	13 (52)	11 (55)	0.70
Oral anticoaglants	9 (20)	4 (16)	5 (25)	0.40
RAS-inhibitors	25 (56)	14 (56)	11 (55)	0.90
Ca-Blocker	15 (33)	10 (40)	5 (25)	0.34
Diuretics	5 (11)	2 (8)	3 (15)	0.42
Beta-blocker	16 (36)	9 (36)	7 (35)	0.95
Oral hypoglycemic agents	15 (33)	7 (28)	8 (40)	0.33

Data are presented as *n* (%), mean ± standard deviation, or median [interquartile range].
BMI, body mass index; BP, blood pressure; BSA, body surface area; Ca, calcium; eGFR, estimated glomerular filtration rate; HDL, high-density lipoprotein; hs-CRP, high-sensitivity C-reactive protein; LDL, low-density lipoprotein; LVEF, left ventricular ejection fraction; NT-pro BNP, N-terminal pro-brain natriuretic peptide; RAS, renin-angiotensin system

Table 3. Relationships between the presence of ruptured plaques and CT and CFD parameters of the aortic arch

	All patients N=45	Presence of Ruptured plaques N=25	Absence of Ruptured plaques N=20	P value
CT findings				
Radius of arch curvature (mm)	30.6±4.3	31.5±4.9	29.5±3.3	0.22
Aortic arch center lumen line length (mm)	144.8±18.2	152.9±20.7	143.7±13.3	0.17
Aortic arch tortuosity index	1.72±0.21	1.72±0.19	1.73±0.24	0.93
Diameter of proximal aortic arch (mm)	33.6±6.2	33.4±6.7	33.8±5.8	0.86
Diameter of distal aortic arch (mm)	26.5±4.1	26.4±3.7	26.7±4.7	0.88
Maximum diameter of aortic arch (mm)	34.3±6.1	34.2±6.4	34.4±6.0	0.94
CFD findings				
Velocity (cm/sec)	83.3±20.3	84.0±15.0	82.4±26.7	0.87
Reynolds number	84.6±26.3	87.6±24.6	80.9±29.6	0.61
Maximum WSS (Pa)				
the whole aortic arch	47.6±28.0	56.2±30.6	36.2±19.8	0.017
at the greater curvature	36.7±23.3	43.2±26.2	28.1±15.8	0.032
at the lesser curvature	43.4±26.9	51.7±29.7	32.5±18.2	0.018
Mean WSS (Pa)				
the whole aortic arch	2.6±0.7	2.6±0.8	2.5±0.6	0.52
at the greater curvature	2.4±0.6	2.5±0.6	2.3±0.5	0.42
at the lesser curvature	2.7±0.9	2.8±1.0	2.7±0.8	0.60

Data are presented as mean ± standard deviation.
CFD, computational fluid dynamics; CT, computed tomography; WSS, wall shear stress
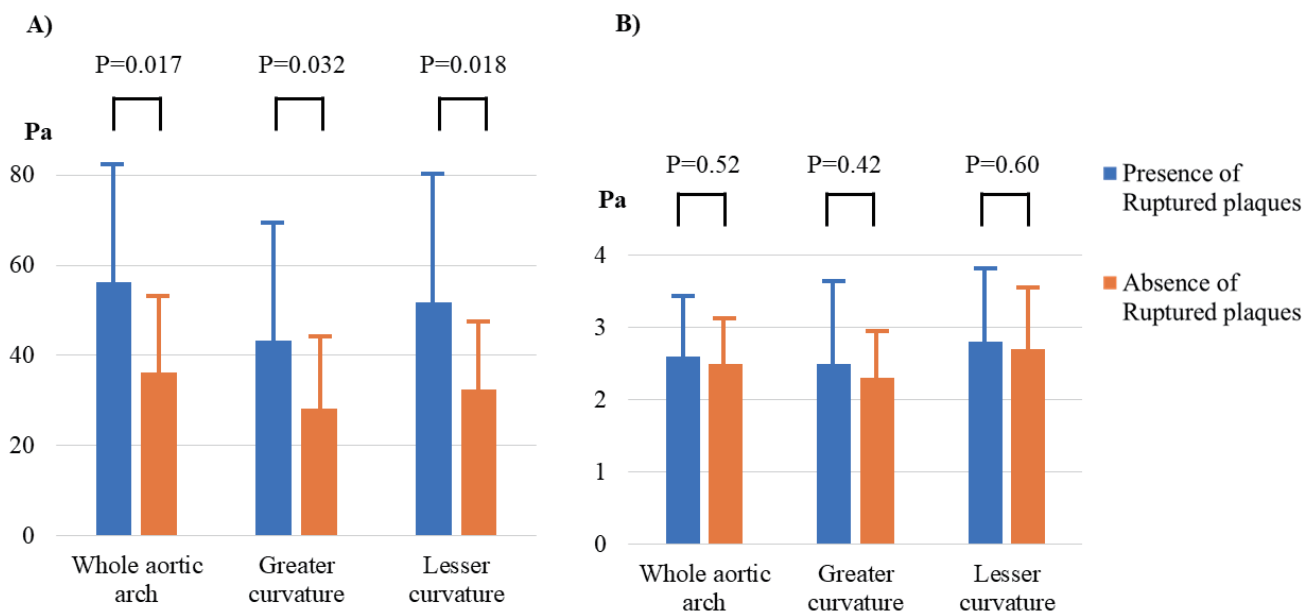
Fig. 2. Relationships between maximum and mean values of WSS and the presence of ruptured plaque in the whole, greater, and lesser curvatures of the aortic arch

(A) maximum WSS; (B) mean WSS. WSS, wall shear stress

Correlation between the Aortic Plaques with NOGA and CFD Findings of the Aortic Arch (Table 4)

The number of RP and thrombi was correlated with the maximum WSS value ($r=0.33$, $P=0.027$; $r=0.32$, $P=0.034$, respectively), whereas the number of RP and thrombi was not correlated with the mean WSS value. Moreover, the maximum yellow grade and

Greater curvature

➢ Max WSS 110.0 Pa

➢ Mean WSS 2.2 Pa

Lesser curvature

➢ Max WSS 30.7 Pa

➢ Mean WSS 1.1 Pa
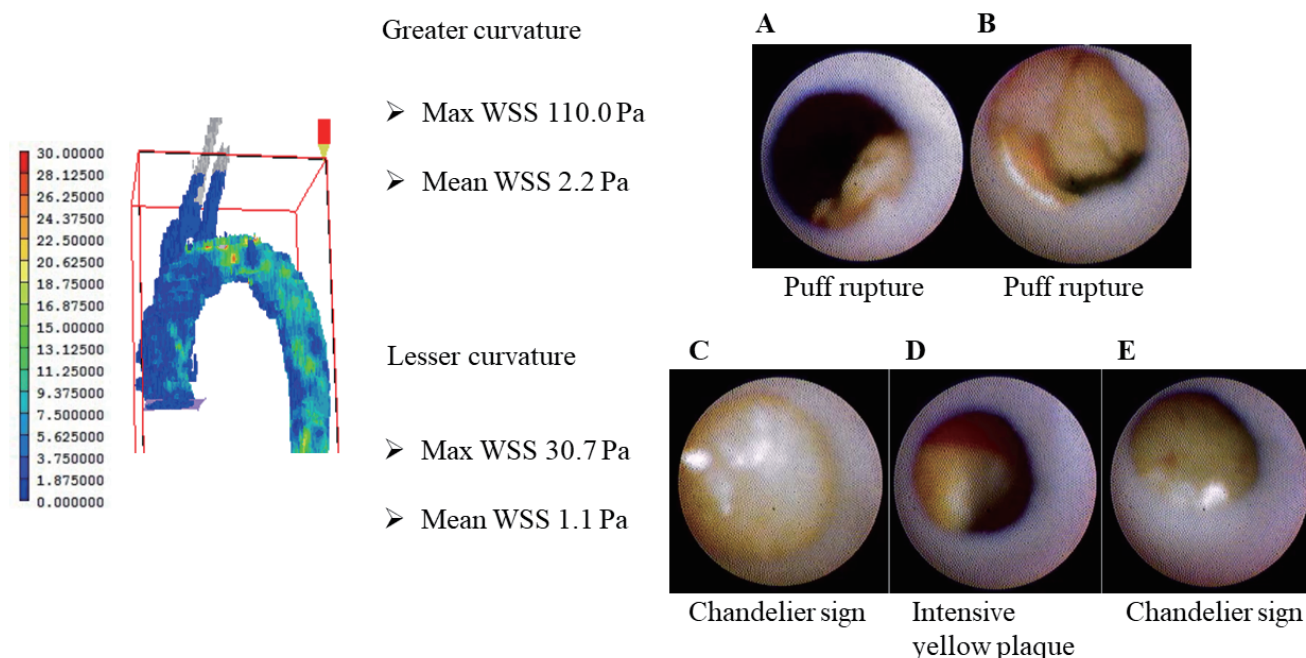
Fig. 3. Representative images of color mapping of WSS and NOGA findings of the aortic arch

A 71-year-old man with hypertension, dyslipidemia, and smoking was admitted to our hospital due to a diagnosis of ischemic heart disease. Coronary arteriography and angioscopy were performed after CT angiography of the aortic arch. The maximum WSS value was higher in the greater curvature than in the lesser curvature. Then, NOGA finding showed aortic ruptured plaques (A, B) in the greater curvature which had much high WSS, although lipid plaques without ruptured plaque (C, D, E) were observed in the lesser curvature with relatively low WSS value. NOGA, non-obstructive general angioscopy; WSS, wall shear stress

Table 4. Correlation between NOGA findings of the aortic arch

	Correlation with Max WSS		Correlation with Mean WSS	
	r	*P* value	r	*P* value
Number of ruptured plaques	0.33	0.027	0.10	0.52
Number of yellow plaques	0.17	0.26	0.02	0.89
Number of thrombi	0.32	0.034	0.004	0.98
Max yellow plaque grade	-0.07	0.65	0.08	0.62

NOGA, non-obstructive general angioscopy; WSS, wall shear stress

the number of yellow plaque were not correlated with both the maximum and mean values of WSS.

Determinants of the Presence of the Aortic RP

The ROC curve for the maximum WSS value predicting aortic RP is shown in **Fig. 4**. The area under the curve was 0.78, and the best discriminate value of the maximum WSS was 42.2 Pa. Then, the maximum WSS value was dichotomized based on these optimal cutoff values. In a multivariate logistic regression analysis, maximum WSS value >42.2 Pa and age were significant predictors of RP detected by NOGA, as shown in **Table 5** (odds ratio 7.21, 95% confidence interval (CI) 1.78–37.1, *P*=0.005; odds

ratio 1.09, 95% CI 1.02–1.19, *P*=0.014, respectively).

Discussion

In this study, we examined the effect of WSS on the presence of RP in the aortic arch evaluated by NOGA in patients who underwent cardiac catheterization. The major findings of this study were as follows: patients with RP within the aortic arch detected by NOGA had a significantly higher maximum WSS value derived by CFD using 3D-CT at the whole aortic arch as well as the greater and lesser curvatures of the aortic arch, and the presence of the maximum
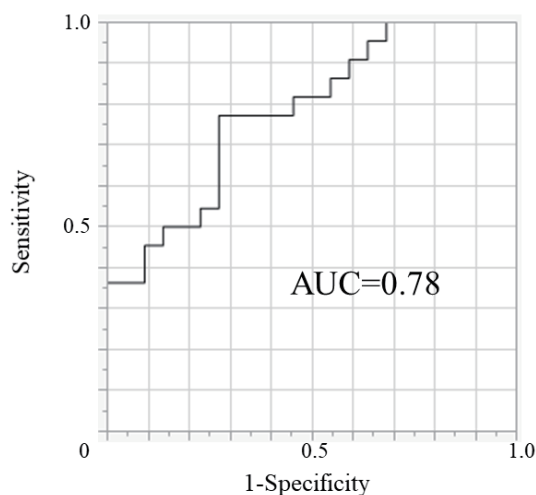
Cut off value	Sensitivity	Specificity
42.2 Pa	77%	73%

Fig. 4. ROC curve for maximum WSS predicting ruptured plaque in the aortic arch

ROC, receiver operating characteristics; WSS, wall shear stress

WSS more than a specific value might be a significant determinant for having a RP in the aortic arch. Furthermore, the number of RP and thrombi was correlated with the maximum WSS value of the aortic arch.

Role of Higher Maximum WSS Value in Aortic RP

Atherosclerotic RP is a dynamic process, in which variable forces onto the vessel wall might be involved in this process. According to the literature, WSS initiates atherosclerosis, and very high WSS value increases the risk of RP[1, 3]. Our findings may support this correlation between high WSS value and RP in the aortic arch level. Fukumoto Y *et al.* reported that localized high shear stress might be a trigger of fibrous cap rupture[3]. They speculated that localized elevation of shear stress involved a significant heterogeneity in endothelial damage and induced a spiral catastrophic cascade leading to RP. According to conventional fracture mechanics, material fracture is frequently initiated at a specific point of stress concentration, which yields a tiny fissure that enhances localized elevation of stress, provoking greater destruction of the structure, like a chain reaction. Although the value

Table 5. Logistic regression analysis for aortic ruptured plaque as maximum WSS value

Variable	Odds ratio	95% CI	*P* value
Univariate logistic regression analysis			
Age	1.06	1.00-1.15	0.049
Diabetes mellitus	1.44	0.42-5.28	0.56
Dyslipidemia	1.43	0.34-6.07	0.62
Hypertension	0.98	0.62-3.53	0.98
Smoke	0.43	0.11-1.44	0.17
Coronary artery disease	1.03	0.29-3.60	0.95
Ischemic stroke	0.43	0.10-1.64	0.22
hs CRP	1.70	0.76-9.98	0.24
LDL-Cholesterol	1.00	0.98-1.02	0.96
HDL-Cholesterol	0.99	0.94-1.04	0.70
Statin	0.92	0.23-3.51	0.90
Aspirin	1.19	0.31-4.41	0.80
Radius of arch curvature	1.06	0.97-1.18	0.20
Aortic arch tortusity index	0.84	0.03-31.6	0.93
Velocity	1.51	0.02-221.5	0.86
Reynolds number	1.01	0.97-1.05	0.58
Maximum WSS (Pa; continuous variable)	1.03	1.01-1.07	0.012
Maximum WSS (>42.2 Pa; categorical variables)	4.60	1.33-17.7	0.016
Mean WSS (Pa; continuous variable)	1.35	0.56-3.55	0.51
Multivariate logistic regression analysis			
Age	1.09	1.02-1.19	0.014
Maximum WSS (>42.2 Pa; categorical variables)	7.21	1.78-37.1	0.005

CI, confidence interval; HDL, high-density lipoprotein; hs-CRP, high-sensitive C-reactive protein; LDL, low-density lipoprotein; WSS, wall shear stress

of blood flow-derived shear stress is usually much less than that of blood pressure-derived tensile stress, higher maximum WSS value might yield a tiny fissure along the inner aortic wall surface that leads to larger destruction of the aortic plaque. Our finding that the mean WSS value was not significantly different between patients with and without aortic RP also suggested that WSS may play a role not on the whole aortic arch but on a specific portion along the aortic wall. The correlation between higher WSS value and aortic RP can also be explained by histological speculation. Previous studies have shown that the vessel endothelium is highly sensitive to hemodynamic shear stresses that act at the vessel luminal surface in the direction of blood flow[2] and that high WSS value induces progression of plaque vulnerability to rupture. High shear stress enhances the expression of vascular endothelial growth factor[24] and induces endothelial nitric oxide synthase, and endothelial nitric oxide mediates shear stress-induced angiogenesis[25, 26]. The new in-plaque vessels promote the accumulation of red blood cells, inflammatory cells, and lipid/lipoproteins within the plaque[27], which subsequently induces intraplaque hemorrhage, necrotic core, and large plaque burden[28], increasing plaque's susceptibility to rupture. Therefore, we can speculate from these suggested mechanisms that the vessel area with higher WSS value is likely to have RP.

Mechanism of Elevation of the Maximum WSS Value within the Aortic Arch

WSS is generated by the friction of blood flow on the endoluminal surface of vessel based on its anatomical features, such as vessel diameter, curvature, and bifurcation, as well as flow profile, especially around the vessel surface[5]. However, this study showed that simple geometric parameters of the aortic arch obtained from 3D-CT, such as vessel diameter and curvature or tortuosity properties, were not significantly related to RP. Furthermore, as shown in representative cases in **Fig.3**, the presence of a plaque that was located in the greater curvature or the lesser curvature did not necessarily determine high or low WSS value. Therefore, more detailed or specific factors might have determined the maximum WSS value. It can be at least speculated that regular observation of the aortic geometry by 3D-CT is unable to assess the susceptibility of the aortic RP, but CFD would be useful to predict it.

Implications for Atheromatous Embolization

Atheromatous embolization from the aortic plaque has been known as one of the causes of ischemic stroke, renal failure, and peripheral arterial disease. Dressler *et al.* used transesophageal echocardiography and showed that patients with systemic embolism who were found to have mobile aortic atheroma had a higher incidence of recurrent vascular events, including ischemic stroke[29]. Desai *et al.* revealed that one of the causes of renal dysfunction is shower embolization of atherosclerotic thrombosis in the renal vasculature[30]. Furthermore, a histopathological study of amputation due to severe limb ischemia reported that the mechanism of the obstructive popliteal artery might be involved in thromboembolism rather than *in situ* thrombosis[31]. Komatsu *et al.* described that NOGA-derived aortic RP which we defined as puff rupture in our study is frequently associated with the spontaneous spread of atheromatous debris, including cholesterol crystal, fibrin, macrophage, and calcification[13, 14], which may induce distal organ ischemia. Furthermore, asymptomatic subclinical atheromatous embolization might cause gradual deterioration of organ function including vascular dementia[32, 33]. Therefore, our CFD analysis of the aortic arch may be useful for predicting future cardiovascular event associated with atheromatous embolization.

Study Limitations

This was a single-center retrospective study with a small sample. Furthermore, some selection bias may exist because we only included patients with cardiovascular disease who underwent 3D-CT as well as cardiac catheterization with NOGA, but our data did not include aortic plaques in patients without cardiovascular disease. This study was performed by two different imaging analyses; however, matching the location examined within the aorta was not completely possible between the two modalities. Therefore, we have compared the data between the two kinds of image areas by area rather than point by point (such as the aortic arch, the greater and lesser curvature) regarding the maximum WSS. We assumed in the CFD analysis that the inflow velocity at the aortic root of the entrance was steady and the same for all patients, although it is actually pulsatile and individually different. However, we considered that the assumption could be overall acceptable for the averaged flow because there were no significant differences between the two groups in cardiac function, blood pressure, and pulse rate at the measurement of WSS. In addition, our study used the other several assumptions to perform CFD analysis, because the actual WSS value cannot be measured in our clinical setting. However, it should be still emphasized that despite this limitation, the calculation of the WSS using our method could provide a useful cutoff value of the maximum WSS value to determine the risk for aortic plaque rup-

ture. Aortic RP has been reported to be related to atherosclerotic risk factors as well as history of coronary artery disease[14]. Furthermore, it was shown that the presence of aortic RP was a risk factor for future cardiovascular events[34]. However, our study did not show any significant difference in the clinical profile between patients with and without aortic RP. One of the reasons may be that both of the study groups had already been well treated for atherosclerosis at the time of examination. It should be rather speculated that even between patient groups matched for the clinical profile, the maximum WSS in the aortic arch might play an important role for provoking aortic RP.

Conclusions

A higher maximum WSS value within the aortic arch derived by CFD using 3D-CT was related to aortic RP detected by NOGA. WSS based on CFD may predict the presence of aortic RP in the aortic arch and future aortic events or even cardiovascular events caused by atheromatous embolization.

Acknowledgements and Notice

None.

Conflict of Interest

The authors have no conflict of interest to declare.

References

1) Kwak BR, Bäck M, Bochaton-Piallat ML, Caligiuri G, Daemen MJ, Davies PF, Hoefer IE, Holvoet P, Jo H, Krams R, Lehoux S, Monaco C, Steffens S, Virmani R, Weber C, Wentzel JJ, Evans PC. Biomechanical factors in atherosclerosis: mechanisms and clinical implications. Eur Heart J, 2014; 35: 3013-3020

2) Davies PF. Hemodynamic shear stress and the endothelium in cardiovascular pathophysiology. Nat Clin Pract Cardiovasc Med, 2009; 6: 16-26

3) Fukumoto Y, Hiro T, Fujii T, Hashimoto G, Fujimura T, Yamada J, Okamura T, Matsuzaki M. Localized elevation of shear stress is related to coronary plaque rupture: a 3-dimensional intravascular ultrasound study with in-vivo color mapping of shear stress distribution. J Am Coll Cardiol, 2008; 51: 645-650

4) Murata N, Hiro T, Takayama T, Migita S, Morikawa T, Tamaki T, Mineki T, Kojima K, Akutsu N, Sudo M, Kitano D, Fukamachi D, Hirayama A, Okumura Y. High shear stress on the coronary arterial wall is related to computed tomography-derived high-risk plaque: a three-dimensional computed tomography and color-coded tissue-characterizing intravascular ultrasonography study. Heart Vessels, 2019; 34: 1429-1439

5) Yamamoto E, Siasos G, Zaromytidou M, Coskun AU, Xing L, Bryniarski K, Zanchin T, Sugiyama T, Lee H, Stone PH, Jang IK. Low endothelial shear stress predicts evolution to high-risk coronary plaque phenotype in the future: a serial optical coherence tomography and computational fluid dynamics study. Circ Cardiovasc Interv, 2017; 10(8). DOI: 10.1161/CIRCINTERVENTIONS.117.005455

6) Stone PH, Saito S, Takahashi S, Makita Y, Nakamura S, Kawasaki T, Takahashi A, Katsuki T, Nakamura S, Namiki A, Hirohata A, Matumura T, Yamazaki S, Yokoi H, Tanaka S, Otsuji S, Yoshimachi F, Honye J, Harwood D, Reitman M, Coskun AU, Papafaklis MI, Feldman CL, PREDICTION Investigators. Prediction of progression of coronary artery disease and clinical outcomes using vascular profiling of endothelial shear stress and arterial plaque characteristics: the PREDICTION Study. Circulation, 2012; 126: 172-181

7) Kumar A, Thompson EW, Lefieux A, Molony DS, Davis EL, Chand N, Fournier S, Lee HS, Suh J, Sato K, Ko Y, Molloy D, Chandran K, Hosseini H, Gupta S, Milkas A, Gogas B, Chang H, Min JK, Fearon WF, Veneziani A, Giddens DP, King 3rd SB, Bruyne BD, Samady H. High coronary shear stress in patients with coronary artery disease predicts myocardial infarction. J Am Coll Cardiol, 2018; 72: 1926-1935

8) Sugimoto K, Shimamura Y, Tezuka C, Tsubota K, Liu H, Okumura K, Masuda Y, Haneishi H. Effects of arterial blood flow on walls of the abdominal aorta: distributions of wall shear stress and oscillatory shear index determined by phase-contrast magnetic resonance imaging. Heart Vessels, 2016; 31: 1168-1175

9) Numata S, Itatani K, Kanda K, Doi K, Yamazaki S, Morimoto K, Manabe K, Ikemoto K, Yaku H. Blood flow analysis of the aortic arch using computational fluid dynamics. Eur J Cardiothorac Surg, 2016; 49: 1578-1585

10) Zarins CK, Xu C, Glagov S. Atherosclerotic enlargement of the human abdominal aorta. Atherosclerosis, 2001; 155: 157-164

11) Seo JS, Lee SY, and Kim HD. Quantitative analysis of aortic atherosclerosis in Korean female: a necropsy study. J Korean Med Sci, 2007; 22: 536-545

12) Mintz GS, Guagliumi G. Intravascular imaging in coronary artery disease. Lancet, 2017; 390: 793-809

13) Komatsu S, Ohara T, Takahashi S, Takewa M, Minamiguchi H, Imai A, Kobayashi Y, Iwa N, Yutani C, Hirayama A, Kodama K. Early detection of vulnerable atherosclerotic plaque for risk reduction of acute aortic rupture and thromboemboli and atheroemboli using non-obstructive angioscopy. Circ J, 2015; 79: 742-750

14) Komatsu S, Yutani C, Ohara T, Takahashi S, Takewa M, Hirayama A, Kodama K. Angioscopic evaluation of spontaneously ruptured aortic plaques. J Am Coll Cardiol, 2018; 71: 2893-2902

15) Kojima K, Kimura S, Hayasaka K, Mizusawa M, Misawa T, Yamakami Y, Sagawa Y, Ohtani H, Hishikari K, Sugiyama T, Hikita H, Takahashi A. Aortic plaque distribution, and association between aortic plaque and atherosclerotic risk factors: an aortic angioscopy study. J Atheroscler Thromb, 2019; 26: 997-1006

16) Marrocco-Trischitta MM, de Beaufort HW, Secchi F, van

Bakel TM, Ranucci M, van Herwaarden JA, Moll FL, Trimarchi S. A geometric reappraisal of proximal landing zones for thoracic endovascular aortic repair according to aortic arch types. J Vasc Surg, 2017; 65: 1584-1590

17) Krams R, Wentzel JJ, Oomen JA, Vinke R, Schuurbiers JC, de Feyter PJ, Serruys PW, Slager CJ. Evaluation of endothelial shear stress and 3D geometry as factors determining the development of atherosclerosis and remodeling in human coronary arteries in vivo. Combining 3D reconstruction from angiography and IVUS (ANGUS) with computational fluid dynam- ics. Arterioscler Thromb Vasc Biol, 1997; 17: 2061-2065

18) Kinlay S, Grewal J, Manuelin D, Fang JC, Selwyn AP, Bittl JA, Ganz P. Coronary flow velocity and disturbed flow predict adverse clinical outcome after coronary angioplasty. Arterioscler Thromb Vasc Biol, 2002; 22: 1334-1340.16

19) Ilegbusi OJ, Hu Z, Nesto R, Waxman S, Cyganski D, Kilian J, Stone PH, Feldman CL. Determination of blood flow and endothelial shear stress in human coronary artery in vivo. J Invasive Cardiol, 1999; 11: 667-674

20) Friedman MH, Bargeron CB, Duncan DD, Hutchins GM, Mark FF. Effects of arterial compliance and non-Newtonian rheology on correlations between intimal thickness and wall shear. J Biomech Eng, 1992; 114: 317-320

21) Krijger JK, Heethaar RM, Hillen B, Hoogstraten HW, Ravens- bergen J. Computation of steady three-dimensional flow in a model of the basilar artery. J Biomech, 1992; 25: 1451-1465

22) Komatsu S, Ohara T, Takahashi S, Takewa M, Yutani C, Kodama K. Improving the visual field in coronary artery by with non-obstructive angioscopy: dual infusion method. Int J Cardiovasc Imaging, 2017; 33: 789-796

23) Hiro T, Komatsu S, Fujii H, Takayama T, Ueda Y, Higuchi Y, Abe S, Kimura S, Kakuta T, Sato A, Matsuoka H, Kawakami H, Ikeda Y, Asakura M, Hayashi H, Yutani C, Saito S, Hirayama A, Kodama K. Consensus standards for acquisition, measurement, and reporting of non-obstructive aortic angioscopy studies: a report from the Working Group of Japan Vascular Imaging Research Organization for Standardization of Non-obstructive Aortic Angioscopy (Version 2017). Angioscopy, 2018; 4: 1-11

24) Gee E, Milkiewicz M, Haas TL. p38 MAPK activity is stimulated by vascular endothelial growth factor receptor 2 activation and is essential for shear stress-induced angiogenesis. J Cell Physiol, 2010; 222: 120-126

25) Goettsch W, Gryczka C, Korff T, Ernst E, Goettsch C, Seebach J, Schnittler HJ, Augustin HG, Morawietz H. Flow-dependent regulation of angiopoietin-2. J Cell Physiol, 2008; 214: 491-503

26) Kolluru GK, Sinha S, Majumder S, Muley A, Siamwala JH, Gupta R, Chatterjee S. Shear stress promotes nitric oxide production in endothelial cells by sub-cellular delocalization of eNOS: a basis for shear stress mediated angiogenesis. Nitric Oxide, 2010; 22: 304-315

27) Bot I, de Jager SC, Zernecke A, Lindstedt KA, van Berkel TJ, Weber C, Biessen EA. Perivascular mast cells promote atherogenesis and induce plaque destabilization in apolipoprotein E-deficient mice. Circulation, 2007; 115: 2516-2525

28) Eshtehardi P, Brown AJ, Bhargava A, Costopoulos C, Hung OY, Corban MT, Hosseini H, Gogas BD, Giddens DP, Samady H. High wall shear stress and high-risk plaque: an emerging concept. Int J Cardiovasc Imaging, 2017; 33: 1089-1099

29) Dressler FA, Craig WR, Castello R, Labovitz AJ. Mobile aortic atheroma and systemic emboli: efficacy of anticoagulation and influence of plaque morphology on recurrent stroke. J Am Coll Cardiol, 1998; 31: 134-138

30) Desai MY, Kwon DH, Nair D, Mankad SV, Popovic Z, DeCastro S, Nasser HJ, Patel A, Kuvin J, Pandian NG. Association of aortic atherosclerosis and renal dysfunction. J Am Soc Echocardiogr, 2008; 21: 751-755

31) Narula N, Dannenberg AJ, Olin JW, Bhatt DL, Johnson KW, Nadkarni G, Min J, Torii S, Poojary P, Anand SS, Bax JJ, Yusuf S, Virmani R, Narula J. Pathology of Peripheral Artery Disease in Patients With Critical Limb Ischemia. J Am Coll Cardiol, 2018; 72: 2152-2163

32) Ezzeddine MA, Primavera JM, Rosand J, Hedley-Whyte ET, Rordorf G. Clinical characteristics of pathologically proved cholesterol emboli to the brain. Neurology, 2000; 54: 1681-1683

33) Laloux P, Brucher JM. Lacunar infarctions due to cholesterol emboli. Stroke, 1991; 22: 1440-1444

34) Yamaguchi M, Yonetsu T, Hoshino M, Sugiyama T, Kanaji Y, Ohya H, Hada M, Sumino Y, Kanno Y, Hirano H, Yuki H, Horie T, Hamaya R, Usui E, Sugano A, Murai T, Lee T, Kimura S, Fujii H, Hikita H, Kakuta T. Clinical significance of the presence of puff-chandelier ruptures detected by nonobstructive aortic angioscopy. Catheter Cardiovasc Interv, 2019 Nov 9. doi: 10.1002/ccd.28574. Epub ahead of print
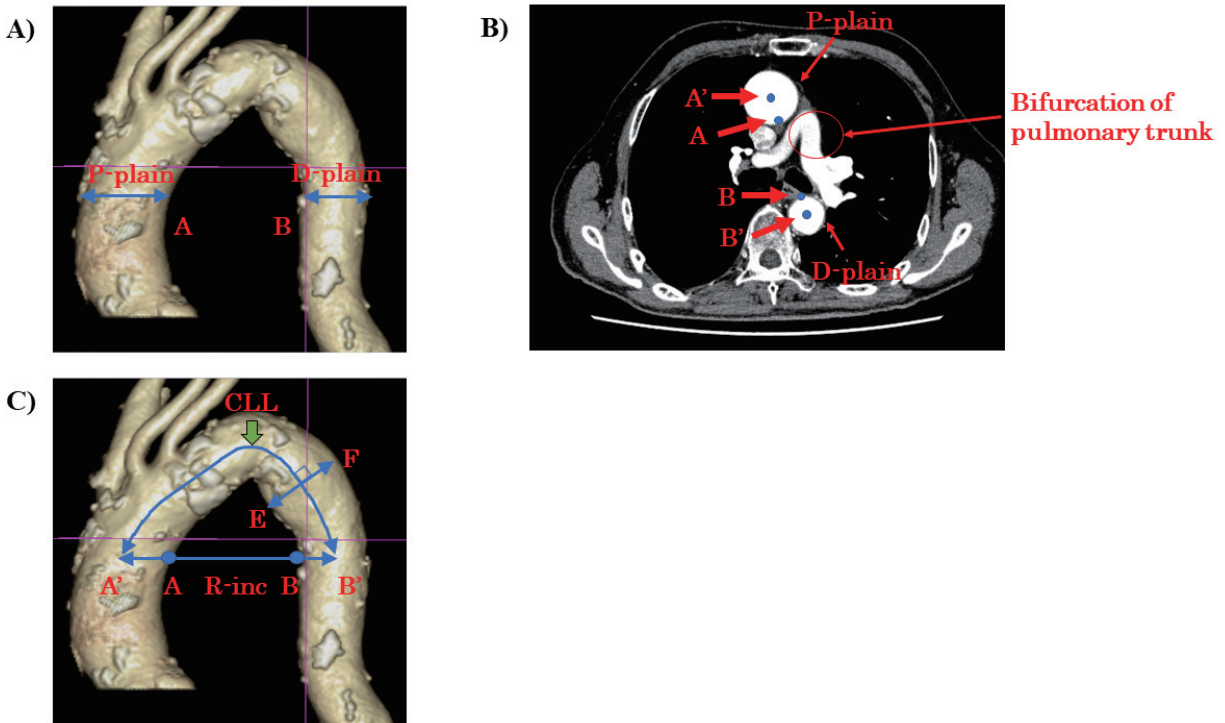
Supplemental Fig. 1. Measurement of CT-derived geometric parameters of the aortic arch of interest

Markers A and B are first determined on the vessel adventitia along the inner curvature of the aortic wall within the same horizontal plane where the distance between the ascending and descending aortas is the minimum at the height of the bifurcation of the pulmonary trunk. Markers A' and B' are the gravity centers of the horizontal luminal cross-section of the ascending and descending aortas (the proximal and distal planes: P-plane and D-plane) within the same plane including Markers A and B. Then, the cross-sectional diameters at P-plane and D-plane are calculated by doubling distances of A-A' and B-B', and the center lumen line length (CLL) is measured along the aortic arch. The radius of the arch curvature (R-inc) is defined as half of the distance between A and B. The aortic arch tortuosity index is defined as CLL divided by R-inc. The maximum diameter of the aortic arch of interest is defined as the maximum lumen diameter perpendicular to the center lumen line.